MEASUREMENTS OF A ROTOR FLOWFIELD AND THE EFFECTS ON A FUSELAGE IN FORWARD FLIGHT

J. G. Leishman*   Nai-pei Bi†

Center for Rotorcraft Education and Research, Department of Aerospace Engineering, University of Maryland, College Park, Maryland 20742, USA.

Abstract - Wind tunnel experiments were conducted to quantify the induced flowfield in the vicinity of a helicopter rotor in forward flight. Tests were performed with an isolated rotor and with a rotor/fuselage combination at advance ratios of 0.075, 0.10 and 0.20. Measurements of the time-averaged total pressure, dynamic pressure and flow angularity were made using an array of miniature seven-hole probes. Data were obtained at a total of 2,688 points in three planes extending below and behind the rotor. The results show that the rotor produces significant increases in total pressure within the boundaries of the rotor wake. The total pressure was distributed in a highly non-uniform manner, both laterally and longitudinally, and was biased primarily towards the rear of the disk. At low advance ratios, the rotor induced velocities were principally downward and produced a download on the fuselage. As the advance ratio was increased however, the induced velocities became quickly streamwise and resulted in an upforce on the fuselage. Considerable changes in the fuselage pitching moments were also obtained due to the relocation of the wake boundaries. The rotor wake boundaries and distribution of induced inflow were only slightly affected by the presence of the fuselage.

Nomenclature

A = Rotor disk area = πR^2

A_1 = Lateral cyclic pitch angle

b = Number of blades

B_1 = Longitudinal cyclic pitch angle

c = Blade chord

C_p' = Pressure coefficient = $100(p - p_\infty)/\frac{1}{2}\rho\Omega^2 R^2$

C_{p_0} = Total pressure coefficient = $(p_0 - p_\infty)/q_\infty$

C_T = Rotor thrust coefficient = $T/(\rho\pi\Omega^2 R^4)$

L = Fuselage length

L_f = Fuselage lift in wind-axis

M_f = Fuselage moment in wind-axis

p = Time-averaged static pressure

p_∞ = Free-stream static pressure

p_0 = Measured local total pressure

q_∞ = Free-stream dynamic pressure = $\frac{1}{2}\rho V_\infty^2$

R = Rotor radius

T = Rotor thrust

V_∞ = Tunnel free-stream velocity

V = Velocity

z_t = Height of probe above floor of tunnel

α_s = Shaft tilt angle (positive aft)

ρ = Air density

σ = Rotor solidity = $bc/\pi R$

θ_c = Collective pitch angle

λ = Rotor inflow ratio = $V_z/\Omega R$

λ_0 = Momentum value of inflow ratio in hover

μ = Advance ratio = $V_\infty \cos\alpha_s/\Omega R$

χ = Wake skew angle= $\tan^{-1}(\mu/\lambda_m)$

Ω = Rotor rotational frequency

*Assistant Professor.

†Graduate Research Assistant.

Introduction

One of the major problems still facing the rotorcraft industry is the lack of information about the flowfield in the vicinity of a rotor in forward flight. This knowledge is necessary to ensure a more thorough understanding of the flowfield environment in which rotorcraft operate, as well as to provide basic data to help validate predictive methods. Furthermore, because all rotorcraft have an airframe situated in close proximity to the rotor, it is imperative to have an adequate understanding of the flowfield about this airframe. Typically, the airframe may comprise non-lifting components, combined with lifting components such as stub wings or tail surfaces. Large effects on overall aircraft performance, as well as the stability and handling qualities, may be experienced at low speeds as a result of the rotor induced inflow acting on both the fuselage and empennage. These effects were first investigated in detail by Sheridan and Smith [1].

The flowfield in the vicinity of a rotor is highly three-dimensional and extremely complicated, the dominant wake structure consisting of strong tip vortices trailed from each blade. The true nature of this wake geometry and the corresponding induced flowfield are still not fully understood, particularly in forward flight. While there have been

extensive measurements conducted to document the wake geometry and induced velocity field for hovering rotors, see for example, Boatwright [2], Landgrebe [3], Caradonna and Tung [4], there is a relative dearth of corresponding information in forward flight. The main reason is that the vortex laden flowfields from a rotor in forward flight are quite intricate, and it is difficult and very time-consuming to obtain measurements of the induced velocities (even time-averaged) at many points in the flowfield at various combinations of rotor thrust, tip path plane angles and advance ratios.

The first comprehensive wake surveys below a rotor in forward flight were performed by Heyson and Katzoff [5]. In these experiments, five-hole pneumatic probes were used to obtain time-averaged local pressures and velocities at large number of points in the rotor flowfield. For many years these data have constituted the most complete and comprehensive available to help validate analytical models of the rotor wake. Other, somewhat more limited, measurements of rotor induced velocities were also obtained by Junker and Langer [6] using five-hole probes. Recently, increasing amounts of data documenting the unsteady flowfield velocities have become available through the use of hot-wire anemometry, e.g. [7], and laser-doppler anemometry techniques, e.g. [8,9]. However, inordinate amounts of wind-tunnel time are generally required with this latter technique, even for one or two components of velocity. This severely restricts the number of points in the flowfield which can be measured during a single tunnel entry. Furthermore, there have been only very limited studies, e.g. [10], in regimes below and behind the rotor where a fuselage and empennage may be located.

While the use of a pneumatic probe does not permit the measurement of instantaneous velocities, the relative ease and speed at which accurate measurements of the mean pressure and three-components of time-averaged velocity can be made at a large number of points in the flowfield, still makes the use of a pneumatic probe an attractive proposition for rotor wake studies. The five-hole probes used by Heyson and Katzoff [5] and Junker and Langer [6] were capable of measuring flow directions up to about 30 degrees relative to the probe axis, see Earnshaw [11]. However, because of the strong vortical nature of a rotor wake, it is not inconceivable that local flow angles can exceed 50 degrees and thereby exceed the practical limits of a five-hole probe.

With the advent of miniature seven-hole probes which can measure flow angularities up to 80 degrees, coupled with recent advances in sensor technology for low pressure measurement, it is now possible to make measurements of flow angle with pneumatic probes to much smaller tolerances and with considerably more certainty. In the present work, miniature seven hole probes are used as a means of quantifying the nature of a rotor wake in forward flight, with and without the presence of a fuselage. The main objective of the work is to comprehensively document the three components of time-averaged velocity in the rotor flowfield, as well as to help explain the effects of the rotor wake on the fuselage airloads. The measurements form part of an ongoing research program at the Univeristy of Maryland [12,13,14] to create a more thorough and comprehensive understanding of rotor/airframe interactional aerodynamics, as well as to create a database which will help validate prediction methods.

Description of the Experiment

The experiments were performed in the Glenn L. Martin wind tunnel at the University of Maryland. This is a closed-return wind tunnel with a 7.75 by 11 foot (2.36 by 3.35 meter) working section. The configuration tested was a 65 inch (1.65 meter) diameter, four bladed rotor. Power to the rotor was supplied by a hydraulic motor, rated at 40 hp (30 kW) @ 6,000 rpm, through a belt transmission. The hub was fully articulated with coincident flap and lag hinges. Each blade was attached to the hub through a pitch bearing. Rotor controls comprised of a conventional swashplate and pitch link mechanism, collective and cyclic pitch angles being set remotely by positioning the swashplate using three electro-mechanical actuators.

The rotor blades were of rectangular planform with a chord of 2.5 inches (6.35cm), and incorporated 12 degrees of nose-down twist. NASA RC(3)10 and RC(4)10 series airfoil sections were used. The blades were constructed of graphite-epoxy with a balsa wood core, and were structurally very stiff relative to a full scale rotor in order to minimize aeroelastic effects. Blade instrumentation comprised strain gauge sensors to monitor bending and torsional loads. Hall-effect sensors located at the hinges were used to monitor the blade flap and lead/lag displacements. Further details of the rotor system are given in [12].

To provide a baseline series of measurements, isolated rotor tests were performed by enclosing the rotor drive mechanism within a minimum body aerodynamic fairing. The remainder of the tests were conducted with a representative helicopter fuselage geometry which consisted of a body of revolution, as shown in Fig. 1. The centerline of the fuselage was located 9.6 inches (24.4cm) below the rotor plane. A summary of the geometric characteristics of the rotor and fuselage are given in Table 1.
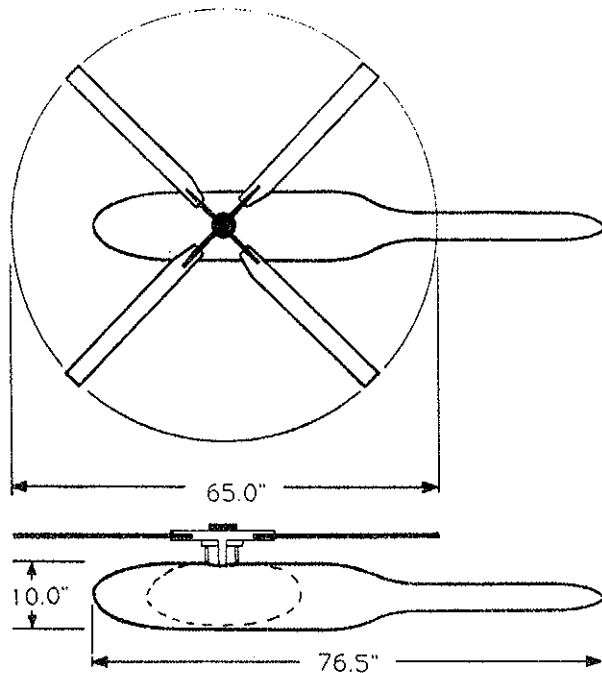
Figure 1: Rotor/fuselage configuration

Table 1: Rotor and fuselage geometry

Number of blades, b	4
Rotor radius, R	32.5 inches (0.8255 m)
Blade chord, c	2.5 inches (0.0635 m)
Rotor solidity, $bc/\pi R$	0.098
Blade twist (linear)	-12°
Blade taper ratio	1.0
Airfoils	NASA RC(3)10/(4)10
Fuselage length, L	76.4 inches (1.94 m)
Fuselage max. diameter	10 inches (0.254 m)
Fuselage taper ratio	2.5:1

Instrumentation

Primary data comprised of measurements of total pressure, dynamic pressure and flow angularity obtained from an array of miniature seven-hole pneumatic probes. These probes were manufactured on-site by packing seven stainless steel hypodermic tubes into a larger stainless steel tube, as shown in Fig. 2. The inner tubes had an inside diameter of 0.028 inches (0.7mm) with a wall thickness of 0.005 inches (0.13mm). Once assembled, the tubes were silver soldered together and machined to provide a 25 degree half angle at the tip. The resulting probes were very small, being about 0.12 inches (3mm) in diameter. Experience has shown that these probes do not significantly disturb the flow they are measuring.

The basic operational principle of the seven-hole probe is to relate measurements of the seven
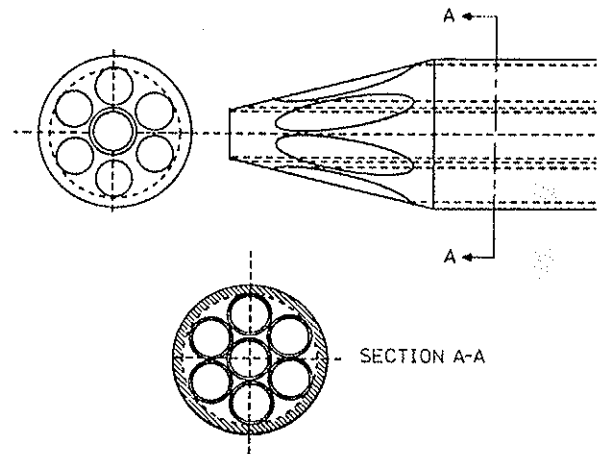
Figure 2: Seven-hole pneumatic probe

port pressures into measurements of total pressure, dynamic pressure and flow angularity. This is achieved through a detailed calibration of the probe in which the port pressures are recorded for known flow angles. For the present work, each probe was individually calibrated in an open jet wind tunnel to pitch and yaw angles of ± 55 degrees. At least 50 data points were taken for each calibration. The calibrations were then curve fitted in a least-squares sense using a fourth order polynomial expansion. Further details of the operational principles of seven hole probes and their calibration procedures is given by Gerner and Maurer [15] and Garner et al. [16]. For the probes used here, the flow angle measurements had a maximum error of 1.0 degrees at low angles ($< 40°$), and at high angles, a maximum error of about 2.0 degrees.

Four probes, spaced 6 inches (15.24 cm) apart, were mounted on a traversing system which was secured to the wind-tunnel floor, as shown in Fig. 3. To ensure that the probes were kept well within the calibration limits (± 50 degrees) when traversing the rotor flowfield, they were pitched at an angle of 30 degrees (in the $x - z$ plane) relative to the tunnel centerline. The probes were traversed in the $x - y$ plane in increments of 3 inches (7.62 cm) using two stepping motors driven by relays under the control of a Hewlett-Packard HP-1000/A900 computer. A program was written to optimize the probe positioning process in order to minimize the number of movements. The probes were traversed over a 28 by 16 point grid on both the left and right hand sides of the rotor flowfield, giving a total of 896 points in one plane, or a total of 2,688 measurement points, as shown in Fig. 4. Three planes were surveyed at heights of $z_t/R = 1.252$, 1.406 and 1.56 above the tunnel floor, or at heights of $z/R = -0.14, -0.29$ and -0.45 relative to the rotor plane.

It should be noted that in all of the tests, the ro-
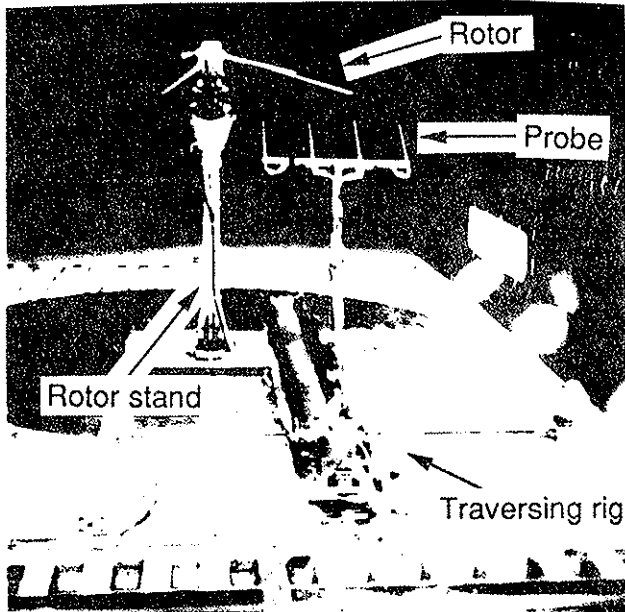
Figure 3: Rotor and traversing system installed in wind-tunnel
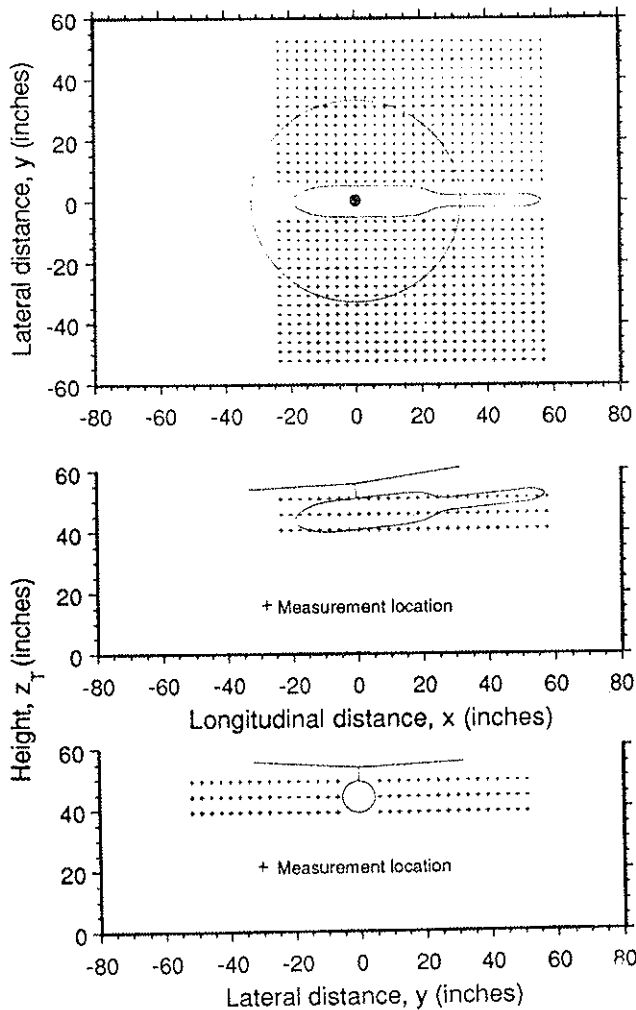
Figure 4: Probe measurement locations

tor tip-path-plane was tilted forward at 6 degrees ($\alpha_s = -6°$). Since the probes were traversed in a plane parallel to the wind-tunnel axis system, the traversing plane was subsequently at a 6 degree angle relative to the rotor tip-path-plane. The probes were brought to within 2 inches (51 mm) of the rotor disk, however, safety considerations did not permit actual measurements up to the leading edge of the disk. Nevertheless, a sufficient number of upstream measurements were still made to identify the leading edge of the rotor wake.

The pressure measurements were made using a Pressure Systems Inc. (PSI) multi-channel Data Acquisition and Control Unit (DACU). The PSI pressure system enabled very low pressures of less than 0.001 lb/in^2 (7.5 Nm^{-2}) to be measured with good accuracy and high repeatability. The pressure ports on the seven-hole probes were connected via short lengths of tubing to a 32-channel PSI pressure transducer module mounted on the traversing system. These modules contained miniature quartz pressure transducers, analog multiplexers and analog to digital converters. A miniature pneumatic valving system in each module also permitted rapid on-line calibration and re-zeroing of the pressure sensors. This capability was essential to maintain measurement accuracy over considerable tunnel run times. Frequent on-line calibrations enabled measurements of the static and dynamic pressures to be made to within a 2% tolerance.

Measurements were also made of the rotor and fuselage loads using independent strain-gauge balances. The rotor hub and controls were suspended from a six component strain-gauge balance which was isolated from the transmission by means of a flexible coupling. Raw balance measurements were passed to an iterative balance subroutine with second-order interaction terms in order to calculate measurements of thrust, side-force, axial force, pitching moment, rolling moment and yawing moment. A separate three component strain-gauge balance was used to measure the normal force, pitching moment and axial force on the fuselage. Deadweight balance tares of the rotor were determined with the blades on and then with them removed. Deadweight tares were also determined for the fuselage. The aerodynamic tares of the hub were determined throughout the advance ratio range with the hub rotating at normal speed, but without the blades attached. Both deadweight and aerodynamic tares have been removed from the balance data presented in this paper.

To complement the fuselage balance loads, time-averaged pressures were also measured at 142 points on the fuselage. Pressure taps were located in rows along the top and on both sides of the fuselage, as shown in [12]. Unsteady pres-

Table 2: Test parameters

Run	θ_c	A_1	B_1	μ	C_T
1	9.93	-4.60	1.54	0.075	0.0074
2	9.74	-5.19	1.37	0.10	0.0075
3	9.59	-5.93	-0.42	0.20	0.0075
4	9.10	-5.30	-0.74	0.075	0.0076
5	9.50	-4.60	0.72	0.010	0.0075
6	9.30	-5.40	-0.85	0.20	0.0075

sure measurements were also made using pressure transducers [12,13,14].

Testing procedures

Data were obtained for the isolated rotor and the combined rotor/fuselage configuration. A single shaft angle of -6 degrees was selected as representative of a helicopter in forward flight. The rotor was run at 1860 rpm (31Hz) for all the tests, which corresponded to a nominal hover tip Mach number of 0.5. For each test, the wind speed was slowly increased while the rotor was "flown" to the desired test condition by adjusting cyclic and collective pitch inputs. At each test point, the rotor was trimmed for the required thrust by adjusting the longitudinal and lateral cyclic to minimize the once-per-rev blade flapping response, thus ensuring that the rotor tip-path-plane was perpendicular to the rotor shaft axis.

After reaching the desired advance ratio, data were recorded by traversing the probes in a plane below and behind the rotor as described previously. Data were acquired at a thrust coefficient (C_T) of 0.0075 and at advance ratios of 0.075, 0.10 and 0.20. An advance ratio of 0.075 was determined to be the lowest possible speed while avoiding significant flow recirculation problems and wall interference effects in the wind-tunnel. This minimum advance ratio was determined from ceiling and sidewall pressure measurements, as well as from tuft observations on the walls and floor of the tunnel. Advance ratios of 0.075 and 0.10 were also selected since they were particularly severe in terms of wake interactions with the fuselage, this being an essential part of the present study. The test conditions and rotor trim parameters are summarized in Table 2. Runs 1, 2 and 3 are for the isolated rotor and runs 4, 5 and 6 are with the fuselage.

A total of 200 measurements of the pressure were made on each port of the probe over a 1.24 second time interval. This corresponded to approximately 38 rotor revolutions and was sufficient time to give a faithful measurement of the mean port pressures for a given point in the flow-field. The time constant for the short length of

tubing between the ports and the sensors was quite small, however, the delay time between the arrival of the probe at a given location and the start of the data acquisition process was conservatively set to 3 seconds to ensure that any transients had died out. Measurements of the port pressures were downloaded in real-time from the DACU to the HP-1000/A900 computer where pressure transducer calibrations were applied and the information recorded on a hard-disk. Further processing was then performed off-line using the probe calibrations to convert the port pressures to measurements of total pressure and three-components of time-averaged velocity. Only data that was within 50 degrees angularity of the probe axis was accepted.

Data were also measured with the hub rotating at normal operating speed, but without the blades, attached in order to give baseline measurements of the flow angularity in the tunnel itself. This also provided some assessment of the induced flow due to the hub. In general, tunnel flow angularities were less than ± 1 degree at all the points measured in these tests. Additionally, hub induced perturbations to the flow were found to be very small, and did not significantly contribute to the measurements. Because of these relatively small effects (at least at the points sampled here), all data presented are uncorrected for tunnel flow angularity or hub effects.

Results and Discussion

Isolated rotor

The isolated rotor tests formed the baseline series of measurements. The total pressure coefficient along the longitudinal direction is shown in Fig. 5 for three planes of the rotor wake, as measured at points closest to the centerline ($y/R = -0.2$), at an advance ratio of 0.075. It is interesting to note that the magnitude of the total pressure was relatively unchanged at each plane. The boundaries of the wake are quite clearly defined, since outside the rotor wake boundaries $C_{P_0} = 1$. Within the wake boundaries, more energy has been added to the flow, and so total pressure coefficients greater than unity are created. Moving aft from the leading edge of the disk higher total pressures are initially obtained, followed by a sudden drop in total pressure to almost free-stream conditions near the center of the wake. This indicates that the rotor has almost zero induced velocity near its center, as would be expected. The highest total pressures are obtained towards the rear of the wake, suggesting that most of the thrust was generated on the rear half (first and fourth quadrants) of the rotor disk.
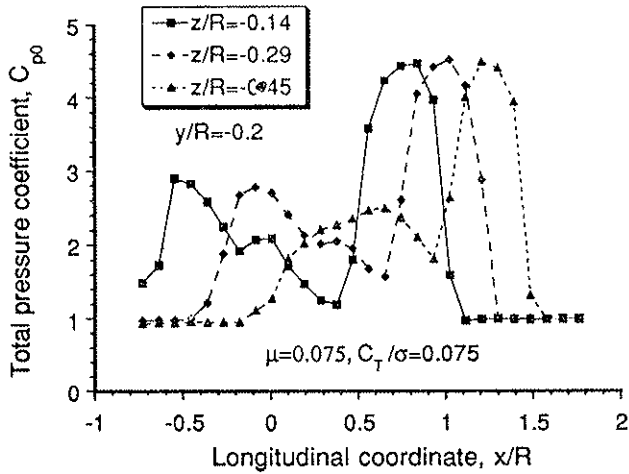
Figure 5: Longitudinal variation in total pressure at three planes below rotor, $\mu = 0.075$

Fig. 6 shows the corresponding longitudinal variation of the x, y and z components of time-averaged velocity (non-dimensionalized with respect to $\Omega R \lambda_0$) for the measurement plane closest to the disk ($z/R = -0.14$), and at advance ratios of 0.075, 0.10 and 0.20. It is interesting that the largest increments in both the x and z components of induced velocity coincide with the largest changes in total pressure in the rotor wake (c.f. Fig. 5). These results confirm the very close correlation between the total pressure in the rotor wake and induced velocity field. As the advance ratio was increased from 0.075 to 0.20, the results showed a reduction in V_z along with a progressive increase in V_x. This is because the main effect of increasing advance ratio (or wind-speed) at a constant rotor thrust, is to increase the skew angle of the wake. At an advance ratio of 0.20, V_z is already close to zero since the wake skew angle is about 80 degrees. Hence, the flowfield velocities are primarily streamwise. The corresponding variations in V_y were found to be relatively small along the longitudinal axis, however, as shown in Fig. 6, there is clearly a significant swirl component in the wake about the hub axis.

The corresponding lateral distribution of total pressure below the disk at $\mu = 0.075$ is shown in Fig. 7 for $x/R = 0.0$, i.e. near the center of the disk, and for each of the three measurement planes. As before, the largest increases in total pressure were obtained towards the edges of the rotor wake. At the highest plane ($z/R = -0.14$), the distribution across the wake was found to be quite dissimilar between the retreating and advancing sides. This is mainly due to the differences in the aerodynamic loading distribution on the retreating and advancing blades; on the retreating blade, the lift distribution is concentrated over the outboard part of the blade, whereas on
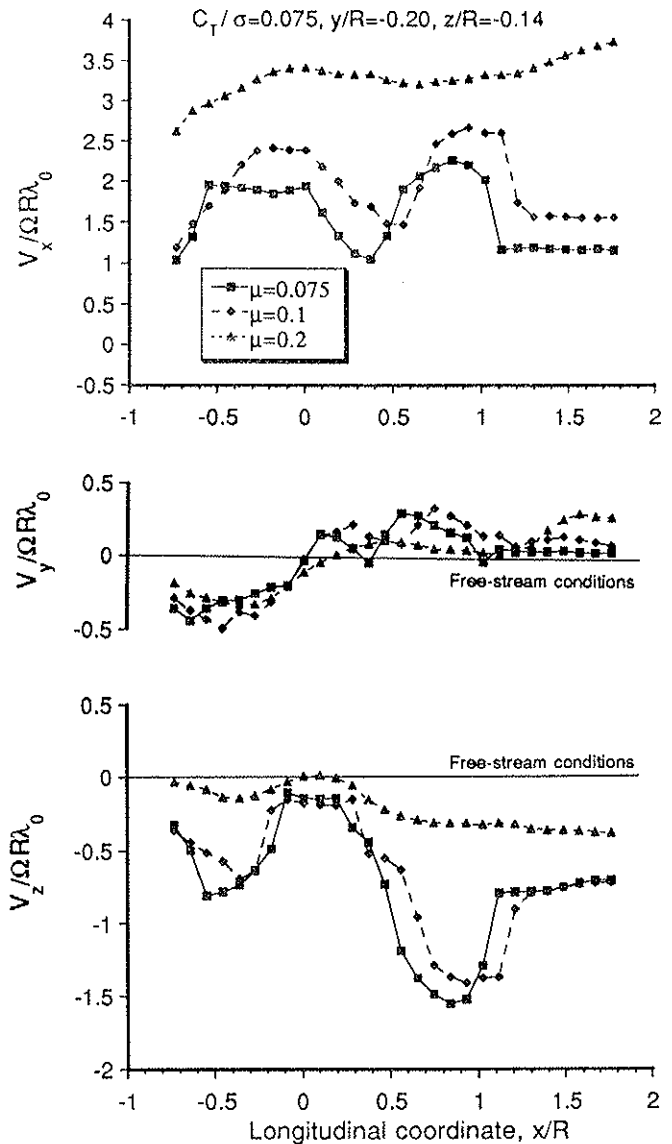
Figure 6: Longitudinal variation in induced velocity below rotor, $\mu = 0.075, 0.10, 0.20$

the advancing blade the lift distribution is somewhat more uniform. Some of the lateral differences in total pressure also occur because the probes are very close to the rotor disk, and are encountering considerably different (time-varying) local wake geometries in the form of both tip vortices and vortex sheets. This can be seen on the advancing side of the disk for $z/R = -0.14$, where the sharp drop in total pressure at $y/R = 0.85$ most likely indicates the presence of discrete tip vortices.

The results in Fig. 7 also indicate the very close correlation of the total pressure in the rotor wake and the lift distribution on the rotor disk. However, it should be noted that this is only true for points very close to the rotor disk where the probes are encountering the actual pressure field about each blade. At points further away from the disk, such as at the intermediate plane
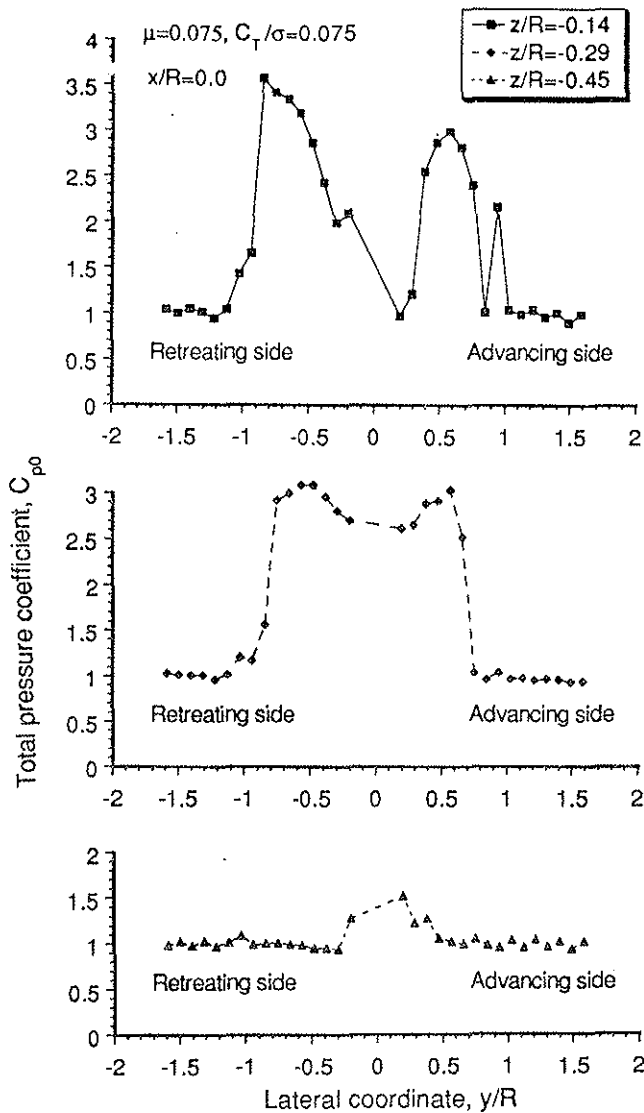
Figure 7: Lateral variation in total pressure at three planes below rotor, $\mu = 0.075$

$(z/R = -0.29)$, it can be seen from Fig. 7 that the distribution of total pressure becomes relatively symmetrical. This is because at this level, the wake structure has rolled up more into discrete tip vortices, and the probes are now far enough away from the rotor such that they are not significantly affected by the local disk loading. It is noteworthy, that a significant contraction of the wake has also occurred at this plane. At the lower planes, the probes encounter progressively less of the wake, and for the lowest plane $(z/R = -0.45)$, only a small region of the leading edge of the wake is actually captured at this longitudinal location.

Whilst the above data are of significant interest and value, a more global picture of the wake structure can be obtained by plotting the total pressure distribution in the rotor wake in the form of contour plots for each of the measurement planes. These data are shown in Fig. 8 for an advance ra-

tio of 0.075. While these data are for the isolated rotor, the outline of the fuselage is also shown for orientation purposes. It can be seen that this form of presentation gives considerable insight into the actual structure of the induced pressure field below and behind the rotor. The highest total pressures in Fig. 8 occur towards the rear of the disk. Specifically, the loadings are higher in the fourth quadrant, where the lift on the blade is concentrated more towards the tip. The highest pressure gradients (closely spaced contours) occur at the boundaries of the rotor wake. In fact, in combination with results such as those in Figs. 5, 6 and 7, it is possible to locate the boundaries of the rotor wake quite accurately. It can be seen from Fig. 8 that there is considerable wake contraction in the longitudinal direction, this being about 78% of the rotor diameter at $0.45R$ below the rotor. However, there is actually a slight expansion of the wake in the lateral direction, this being about 105% of the rotor diameter. Similar results were obtained for an advance ratio of 0.10, however, at an advance ratio of 0.20, the wake skew angle was already too high to accurately define the wake boundary.

Regions of both very high and very low total pressure occurred downstream in the "far" wake of the rotor. Again, as shown in Fig. 8, the contours are closely spaced, indicating that the downstream wake still has a very definite boundary. A very concentrated region of high dynamic pressure was formed on the advancing side of the wake. This is due to the relatively large induced velocities created by the tip vortices from each of the rotor blades as they interact and produce a self distorting rolled-up bundle of vortices just downstream of the disk. Regions of very low dynamic pressure also occurred downstream of the retreating side of the disk, however, the distribution in the wake was notably different from the advancing side. This is because of the fundamental differences in wake geometry and induced velocity field between the advancing and retreating sides of the disk. It is interesting that there also appears to be certain amount of lateral expansion of the wake boundary at the lower measurement planes as it develops downstream of the disk. This process is discussed again later in this paper.

Effects of the fuselage on rotor

On the whole, the effects of the fuselage on the flowfield measurements were found to be quite small. Despite these small differences however, it should be noted that the repeatability of the data from test to test was extremely good. Thus, the differences which are attributed here to the effects of the fuselage on the rotor flowfield are presented with a high degree of confidence.

z/R=-0.14

z/R=-0.29

z/R=-0.45
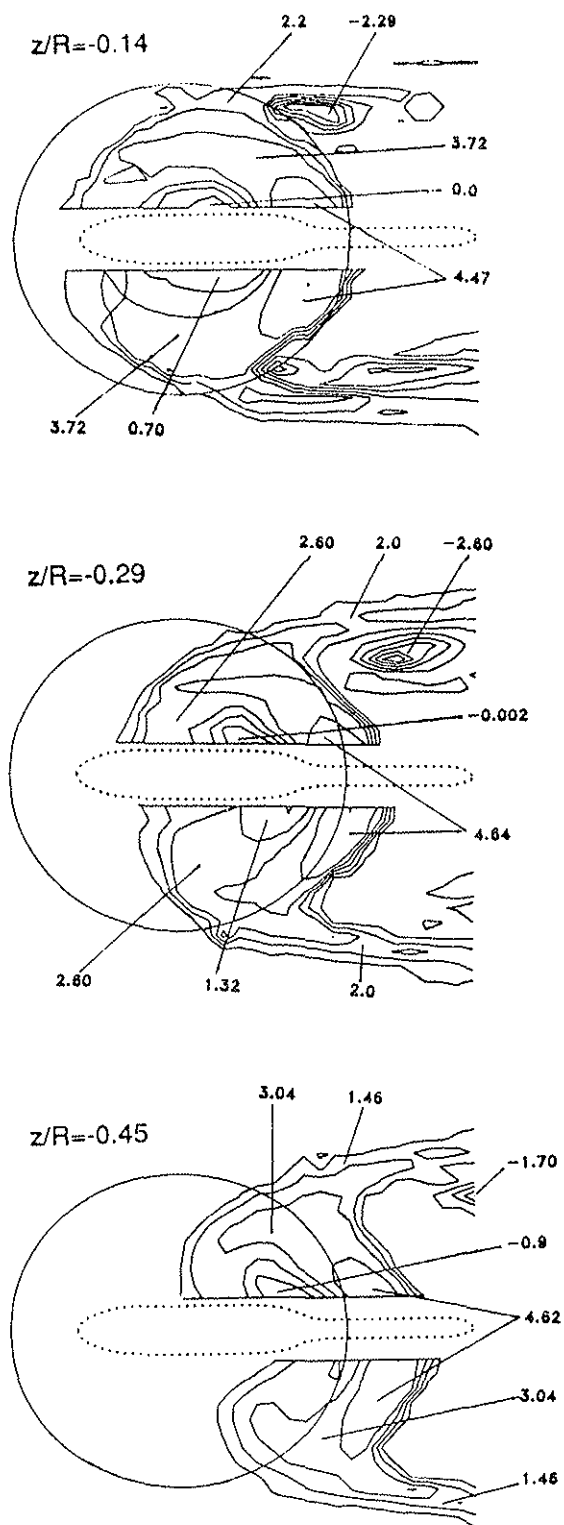
Figure 8: Total pressure contours in rotor wake, $\mu = 0.075$

$\mu=0.075$, $C_T/\sigma=0.075$, $y/R=-0.20$, $z/R=-0.29$

Free-stream conditions

— ■ —Isolated rotor
– ◆ –Combined rotor/fuselage

Free-stream conditions
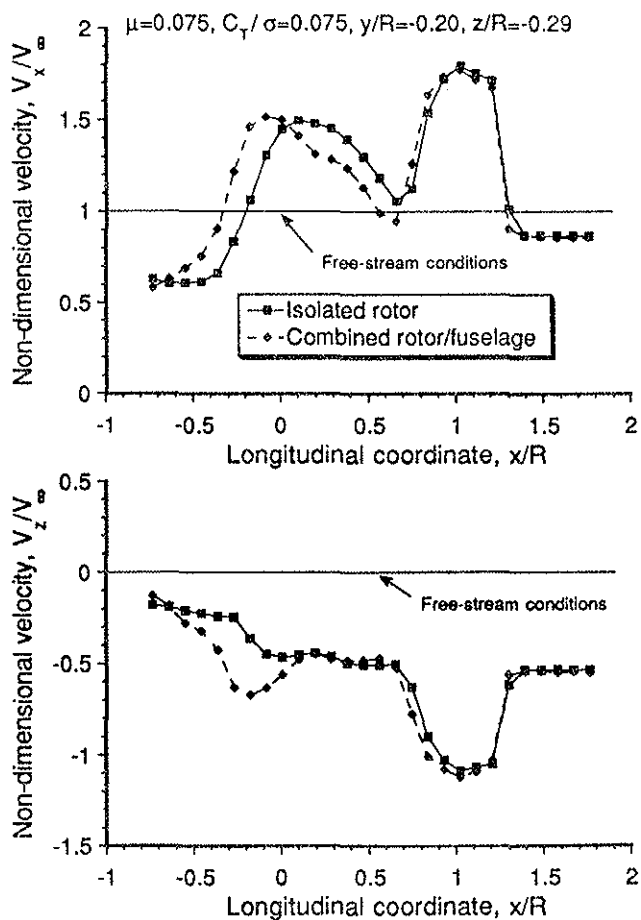
Figure 9: Wake velocity distribution with and without fuselage, $\mu = 0.075$

Away from the immediate vicinity of the fuselage, both the total pressures and flow angularities were almost identical to their isolated rotor counterparts, as shown in Fig. 9. Some differences in the flowfield velocities were found to occur near the nose of the fuselage for an advance ratio of 0.075, however, as the advance ratio was increased, these differences significantly diminished. By way of example, the x and z components of wake velocity (non-dimensionalized by the free-stream velocity) in the middle plane ($z/R = -0.29$) along the longitudinal direction nearest to the fuselage ($y/R = \pm 0.2$) are shown in Fig. 9 for $\mu = 0.075$. The effect of the fuselage appears to increase V_x upstream of the hub region compared to the isolated rotor values. Downstream of the hub, V_x is a little less, and eventually there are no measurable differences over the rear fuselage region.

These above results are more or less what is to be expected, since in forward flight the fuselage must accelerate the flow over nose region, followed by a deceleration of the flow over the tapered region ($x/R \approx 0.7$). This is followed by a gradual increase in flow velocity over the tail boom back to free-stream conditions. Hence, the main effects

on V_x should only be apparent over the front part of the fuselage, as it appears to be. The presence of the fuselage was also found to increase the magnitude of the vertical velocity, V_z, in the vicinity of the nose region. Immediately above the fuselage, V_z must be less than that for the isolated case, although at the sides (where the measurements are taken) the flow from the rotor wake is accelerated over the sides of the fuselage and consequently, the flowfield velocities are a little greater in these regions.

Thus, from the foregoing it appears that to a first order, it may be possible to neglect the changes in the induced velocity field due to the distortion of the rotor wake by the fuselage. This however, does not imply that the rotor wake geometry and rotor performance are unaffected by the presence of the fuselage, as it certainly is. For example, Table 2 shows that when the body is present, lower collective pitch angles are required compared to the isolated rotor case for a given value of thrust. This is particularly evident at the lower advance ratios, and is discussed further in [12,13]. Furthermore, recent research has shown that major distortions to the wake are produced by the fuselage, especially in regions of wake impingement. Such details of wake distortion due to the fuselage are currently under study [14], but are beyond the scope of the present paper.

Effects of rotor on fuselage loads

The effects of the rotor wake on the airframe loads are a serious cause for concern on all modern rotorcraft. The current trend to design more compact helicopters, means higher disk loadings, which consequently give rise to more energetic wakes and higher induced velocities. Besides producing significant downloads on the airframe at low speeds, this induced velocity field may also produce airloads which vary in a complex manner under different flight conditions, and thereby may produce major effects on the handling qualities of the aircraft.

For the present configuration, the measured pressure distributions along the top and on the two sides of the fuselage are shown in Fig. 10 for advance ratios of 0.075 and 0.10. These particular data are presented as pressures nondimensionalized with respect to rotor tip speed, ΩR, which is denoted by C_p'. It should be noted that this is different from the classical definition of pressure coefficient which is based on V_∞. Using C_p' is appropriate here since it gives a much better indication of the actual pressure on the fuselage for comparison purposes at different advance ratios.

In general, Fig. 10 shows that the rotor wake had a very pronounced effect on the fuselage pressure distribution, especially at the lower advance
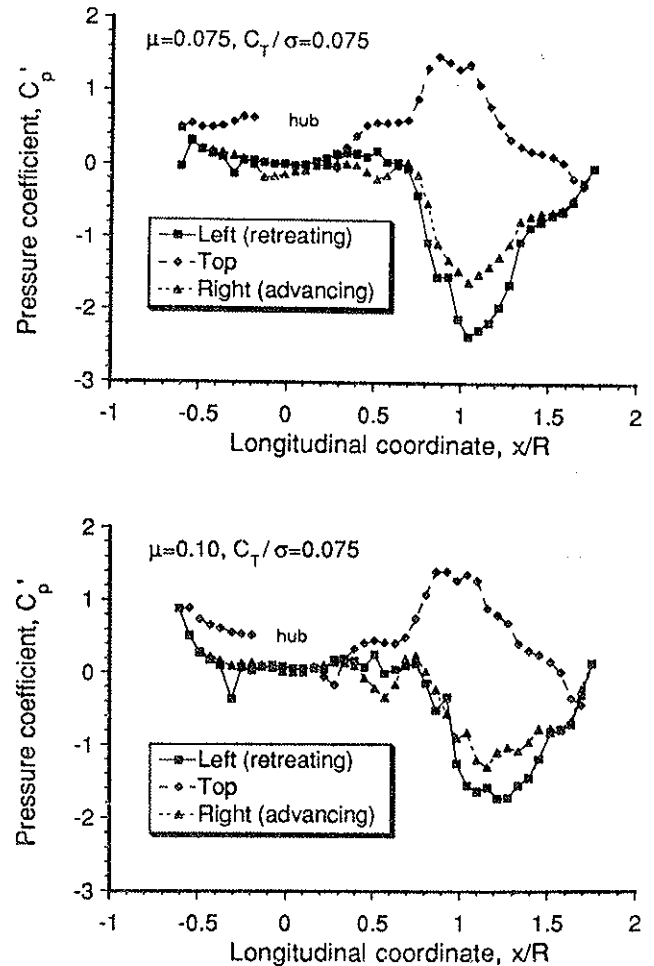
Figure 10: Pressure distribution on top and sides of fuselage, $\mu = 0.075, 0.10$

ratios. Significant increases in pressure were obtained over the top of the fuselage in regions affected by the rotor wake. On the sides of the fuselage, large suction peaks were generated as the induced flow accelerated over the sides of the fuselage. As the advance ratio was increased, these peaks moved aft on the fuselage since the wake skew angle becomes greater. It should be noted that the high adverse pressure gradient downstream of the suction peak means that the boundary layer on the fuselage may be very susceptible to separation compared to the isolated fuselage case. The corresponding pressure distribution over the isolated fuselage is given in [12].

Another aspect of the pressure distributions shown in Fig. 10, is that the distributions on the two sides of the rear fuselage are different, with a higher suction pressure being obtained on the left side of the tailboom. This indicates that the fuselage will experience both a side force (to port) and a yawing moment (nose right). On an actual helicopter, this may be important from a handling qualities perspective. A similar result has been also noted by Wilson and Mineck [17]. While the magnitude of the side force and yawing moment
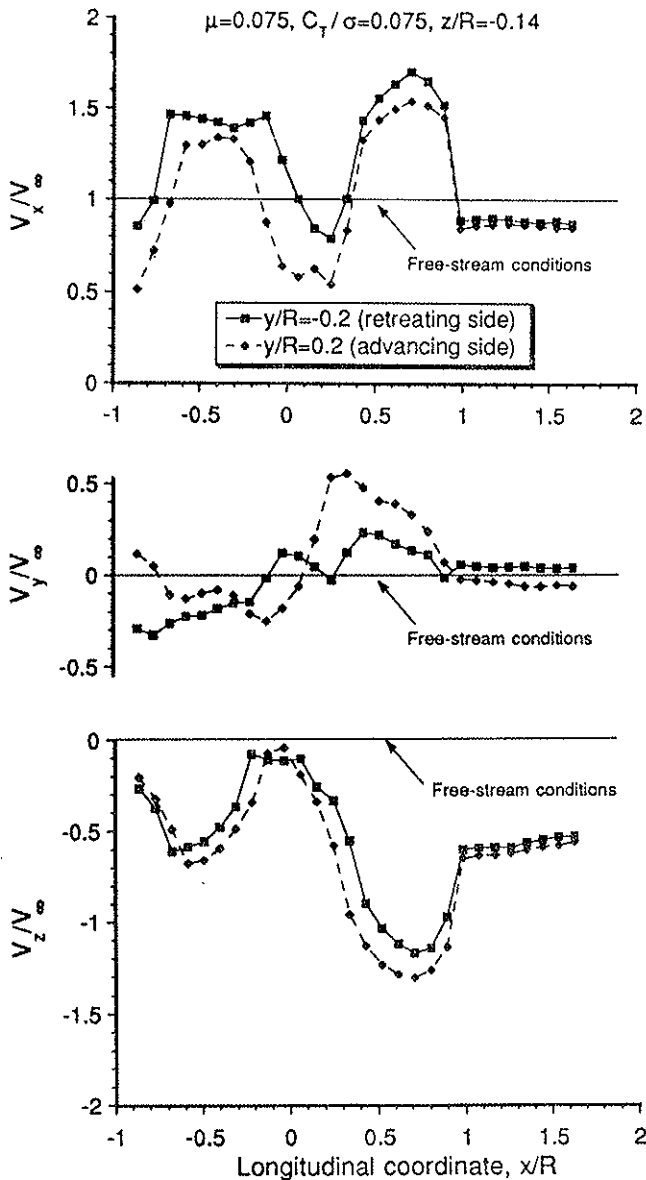
Figure 11: Three-components of induced velocity in rotor wake, $\mu = 0.075$

was not measured in the present experiments, the source of the pressure differential on the rear fuselage is certainly of significant interest.

The three components of the flowfield velocity (non-dimensionalized with respect to the tunnel free-stream velocity) on the right and left hand sides of the fuselage ($y/R = \pm 0.2$) are plotted in Fig. 11. It can be seen that the downwash (V_z) is one of the most significant velocity components, this being a little higher on the right hand (advancing) side of the fuselage. Clearly this component alone cannot explain the measured pressure differential on the fuselage, since the relative velocity would be expected to be higher on the left hand side. In any case, the variation in V_z across the width of the fuselage is too small to account for the measured pressure differences.

The magnitude and sign of V_y also indicates

that there is small crossflow velocity component (from the retreating side to the advancing side), the crossflow angle being roughly 15 degrees. Potential flow theory predicts that this crossflow velocity will not produce a difference in pressure between the left (retreating) and right (advancing) sides of the fuselage. On the other hand, a viscous theory predicts a higher suction pressure on the left side of the fuselage as a consequence of flow separation on the right side of the fuselage. At low advance ratios, this particular fuselage will act like a slender body at an angle of attack, and may produce a wake in the form of a vortex system on the lee-side. This vortex system may, in fact, be either stable or periodic. During some of the tests, a certain amount of buffeting was recorded on the fuselage balance loads, hence it is likely that the lee-wake was periodic. Nevertheless, in either case, the presence of a wake on the lee-side of the fuselage will affect the fuselage pressure measurements, and should be considered as a contributing factor to the results shown in Fig. 10. Further details of the fuselage wake is currently under study using laser sheet/smoke flow visualization. Thus, the crossflow velocity appears to be, at least partially, responsible for the measured pressure differential on the rear fuselage.

In addition to the crossflow velocity, there is a significantly higher streamwise velocity (V_x) in the fourth quadrant of the rotor wake, as also shown in Fig. 11, and is slightly higher on the retreating side of the disk. Interestingly, this component must also be responsible for part of the pressure differential on the rear fuselage. In fact, it is significant to note the very substantial variations in V_x along the whole longitudinal axis of the rotor wake. These variations are, in some locations, as much as 50% of the free-stream velocity and will certainly contribute to the fuselage pressure distribution and loads. As in the case of the downwash, V_z, the highest variations in V_x also occur in regions of highest total pressure. Thus, in any predictive method for rotor wake/fuselage interaction effects, it may be necessary to compute all three components of the rotor induced velocity field in order to give accurate predictions of the pressures and resultant airloads on the fuselage.

The velocity vectors below the rotor are shown in Fig. 12 for an $x - z$ plane at $y/R = -0.2$. It can be seen that for all three advance ratios the induced velocities are greatest towards the rear of the rotor wake. In these figures, the wake boundaries have also been included, as inferred from Figs. 5 through 8. It is significant that the leading edge of the wake has a much higher skew angle than the rear of the wake. This is because the highest induced velocities are biased towards the rear of the disk, and hence the ratio $\mu\Omega R/V_z$ is much smaller in these regions. It is of interest to
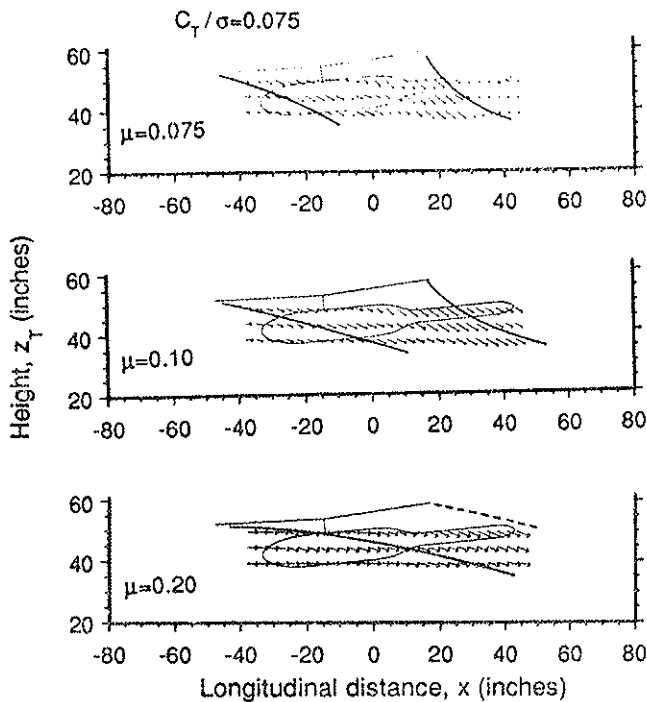
Figure 12: Induced velocity vectors and wake boundaries

note the high sensitivity of the wake skew angle to changes in the advance ratio. Compared to the isolated rotor case, the wake boundary was found not to be significantly affected by the presence of the fuselage.

As also shown in Fig. 12, for advance ratios of 0.075 and 0.10, both the leading and trailing edges of the wake appear to directly impinge on the fuselage. Thus, there will be significant wake/fuselage interactions at these advance ratios. At the highest advance ratio of 0.20 the wake skew angle is close to 80 degrees, and no significant wake impingement occurs on the fuselage. Nevertheless, this is not to say that the rotor wake does not interact with the fuselage at this advance ratio. According to Fig. 12 there is a region of fairly high induced velocities which are primarily streamwise and are confined to regions directly above the top of the fuselage. This actually produces more of a suction pressure on the top of the fuselage, as opposed to the stagnation pressures obtained at lower advance ratios. There are also additional unsteady effects on the fuselage loads which must be considered at all advance ratios, as discussed in detail in Ref. 12.

The corresponding effects of the rotor wake on the fuselage lift and pitching moment are shown in Fig. 13 as a function of advance ratio. The isolated fuselage values for all advance ratios at this shaft angle were close to zero. It should be noted that the results in Fig. 13 are given in terms of dimensional units. This is necessary, since if standard coefficient values are used, the effect of
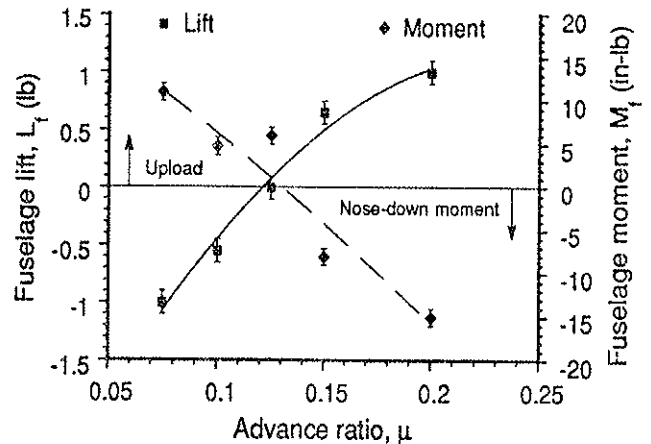
Figure 13: Fuselage lift and pitching moment variation with advance ratio

increasing μ is to decrease the coefficient values for a constant lift, and so this may produce misleading trends when interpreting the interactional loads. It can be seen from Fig. 13 that the rotor provides a significant download on the fuselage at low advance ratios. As the advance ratio is increased the download becomes much less, and at the highest advance ratio of 0.20 an upforce is actually obtained. This essentially reaffirms the results presented by Smith and Betzina [18]. At the same time, Fig. 13 shows that the fuselage pitching moment decreases (a nose-down moment) with increasing advance ratio. This indicates that the rotor wake modifies the pressure distribution on the fuselage in such a way as to move the center of pressure further aft, as shown previously in Fig. 10. It should be noted that data points at advance ratios of 0.05, 0.125, 0.15 are included in Fig. 13 even though flow surveys were not performed at these conditions.

Wake aft of rotor disk

Downstream of the rotor disk, the wake was found to roll-up very quickly to form into two major tip vortices. This process was found to be unaffected by the presence of the fuselage. The wake roll-up process behind a rotor was first observed by Heyson [19], and is in fact very similar to that obtained from a low aspect ratio wing. This can be readily seen in Fig. 14 where the induced velocity vectors at $\mu = 0.075$ are plotted for two $y - z$ planes downstream of the rotor disk at $x/R = 1.05$ and 1.51. It is interesting that the wake roll up process starts to occur almost immediately downstream of the disk. At $x/R = 1.51$, the velocity vectors indicate that the wake has almost completely developed into two predominant vortices. These "far wake" vortices will consist of the rolled-up remnants of the tip vortices trailed from each blade. This figure also shows that the
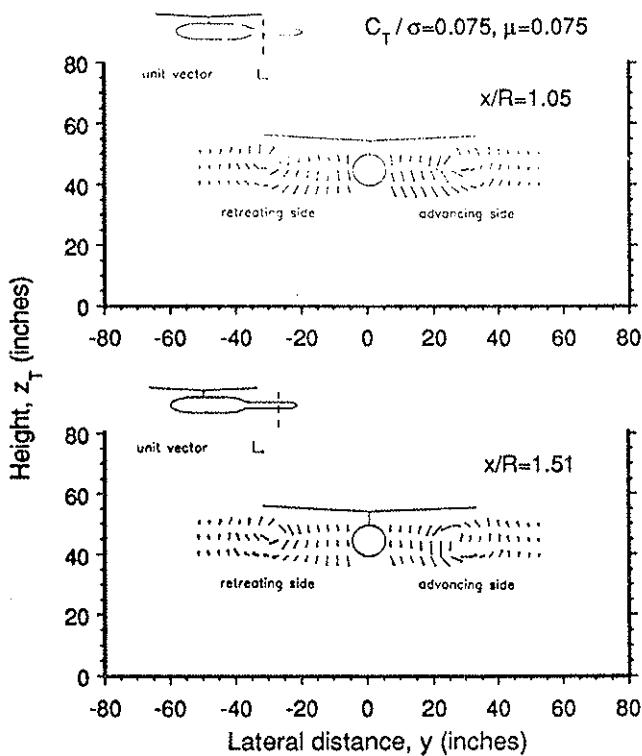
Figure 14: Induced velocity vectors in wake downstream of rotor, $\mu = 0.075$

Figure 15: Total pressure variation in far wake, $\mu = 0.075$

centroid of the trailed wake vortex bundles are located near the edges of the disk. However, the trajectory of the wake boundary still indicates a gradual expansion downstream, as shown previously in Fig. 8. It is also significant that these well-developed wake vortices are trailed almost streamwise behind the rotor, in contrast to the center of the wake which has a much smaller skew angle.

The wake roll up process can be further supported from the lateral measurements of total pressure and induced velocity. These data are plotted in Figs. 15 and 16 respectively for the middle plane ($z/R = -0.29$). It can be seen from Fig. 15, that there are very large changes in total pressure in the vicinity of the two wake vortices. Away from the wake vortices, the total pressure returns to almost free-stream conditions. At $x/R = 1.05$ the probes are still within the boundary of the main wake for $-0.5 \leq y/R \leq 0.5$, and hence higher total pressures are obtained at these points. Similar results were obtained for $\mu = 0.10$ and 0.20, although the wake roll-up starts to occur a little further downstream for these latter conditions.

In Fig. 16, the induced velocity (V_z) gradient was found to be fairly small across the rear fuselage for both $x/R = 1.05$ and $x/R = 1.51$. However, it is clear that the downwash is higher on the right (advancing) side of the disk. This is because the wake rolls up somewhat more quickly on the

advancing side, and so the induced velocity field on this side becomes stronger closer to the disk. The downwash velocity field for $x/R = 1.51$ is, in fact, almost identical to what would be obtained from two vortices of just slightly different strength which are trailed from the rotor. It should be noted that on an actual helicopter with a horizontal stabilizer located in the rear fuselage region, this would produce a coupling of pitch with sideslip as the stabilizer moves into the higher downwash on the advancing side or to the somewhat lower downwash on the retreating side. A further discussion of this effect is given by Cooper [20].

In the present work, it was found that flow angularities of 40 to 50 degrees (relative to the probe axis) existed in many parts of the flowfield aft of the disk. While these measurements are certainly within the capabilities of the seven-hole probes used here, it makes the results from other measurements of rotor flowfields with five-hole probes a little questionable, since five-hole probes typically have a maximum angularity measurement of less than 30 degrees. For example, in this experiment the induced flow angles in the vicinity of the

$\mu{=}0.075,\ C_T/\sigma{=}0.075,\ z/R{=}-0.29$

Free-stream conditions

Free-stream conditions

—■—x/R=1.05
– ◇ –x/R=1.51
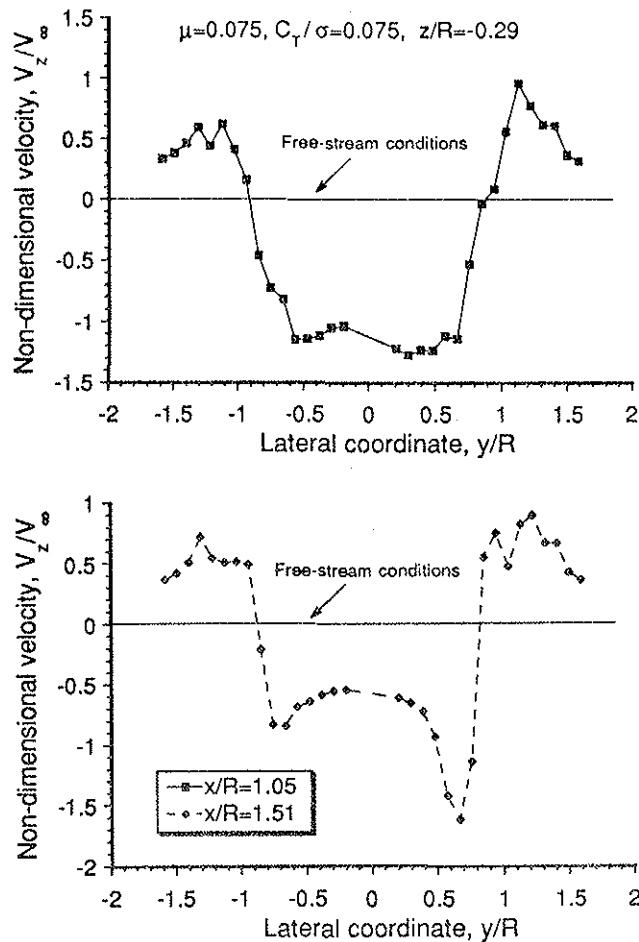
Figure 16: Induced downwash variation in far wake, $\mu = 0.075$

rear fuselage were such that the angles of attack (relative to the fuselage centerline) in these regions varied from about 60 degrees at $\mu = 0.075$ to 10 degrees at $\mu = 0.20$; corresponding yaw angles ranged up to as much as 30 degrees. This information would be very important in determining the location and orientation of either a horizontal or vertical stabilizer on a helicopter fuselage, especially during transition from hover to forward flight, or when operating in a side-slip. Currently, very little is known about either the time-averaged or the unsteady velocity field in the vicinity of an empennage. Further experiments must be done to more fully understand these effects.

Conclusions

A study has been conducted to quantify the induced flowfield in the vicinity of a helicopter rotor in forward flight. Tests were performed with an isolated rotor and with a rotor/fuselage combination. The seven-hole pneumatic probe was shown to be a very effective means of measuring the time-averaged induced velocity field. An extensive map of the time-averaged induced velocities in the rotor flowfield was obtained at three advance ratios

in three planes at a total of 2,688 points. These data have provided an improved understanding of the induced flowfield environment encountered by a fuselage in forward flight. The results can also be used to compare with analytical models of the rotor wake induced velocity field, and with predictions of rotor/fuselage interactional effects. Furthermore, these data have been useful in providing guidance in selecting regions of the flowfield for further and more detailed study using hot wire anemometry and/or laser-doppler velocimetry techniques.

The following conclusions have been drawn from the present work:

1. The rotor produced significant increases in total pressure and high induced velocities within the boundaries of the rotor wake. These distributions varied in a highly nonuniform manner, both laterally and longitudinally, and were biased primarily towards the rear (first and fourth quadrants) of the disk.

2. The rotor wake boundaries and distribution of induced inflow were only slightly affected by the presence of the fuselage, however measurable changes in rotor performance were still obtained. When the fuselage was present, lower values of collective pitch were required for a given value of rotor thrust.

3. At low advance ratios, the rotor induced velocities were primarily downward and resulted in a download on the fuselage. As the advance ratio was increased, the induced velocities became quickly streamwise and produced an overall upforce on the fuselage. At the same time, significant fuselage pitching moments were obtained due to the relocation of the wake boundaries.

4. There was a significant differential pressure on the rear fuselage, which appeared to be due to a certain amount of crossflow. There were also very substantial variations in streamwise velocity along the whole longitudinal axis of the rotor wake. These variations were, in some locations, as much as 50% of the free-stream velocity and may significantly contribute to the fuselage pressure distribution.

5. There was considerable wake contraction below the rotor at all the advance ratios measured. The wake contracted longitudinally to some 78% of the rotor diameter within $0.45R$ below the rotor. However, there was actually a slight expansion in the lateral direction, this being about 105% of the rotor diameter.

6. The rotor wake was found to roll up quickly behind the disk to form two major trailing tip vortices of almost equal strength. The

wake from the advancing side of the disk was found to roll-up more rapidly than the wake from the retreating side, however both vortices were trailed almost streamwise behind the rotor disk.

References

1. Sheridan, P.F., Smith, R.P., "Interactional Aerodynamics - A New Challenge to Helicopter Technology," Pre-print No. 79-59, Presented at the *35th Annual Forum of the American Helicopter Society*, Washington D.C., May 1979.

2. Boatwright, D.W. "Measurements of Velocity Components in the Wake of a Full-Scale Helicopter in Hover," USAAMRDL TR 72-33, 1972

3. Landgrebe, A.J., "An Analytical and Experimental Investigation of Helicopter Rotor Performance and Wake Geometry Characteristics," USAAMRDL TR 71-24, 1971

4. Caradonna, F.X., Tung, C., "Experimental and Analytical Studies of a Model Helicopter Rotor in Hover," Paper No. 4, *7th European Rotorcraft Forum*, Garmisch-Partenkirchen, F.R.G., Sept. 1981.

5. Heyson, H. H., Katzoff, S. "Induced Velocities Near a Lifting Rotor with Non-Uniform Disk Loading," NACA TR 1319, 1957.

6. Junker, B., Langer, H.J., "Helicopter Rotor Downwash: Results of Experimental Research and Comparison with some Theoretical Results," *Vertica*, Vol. 7, No. 1, 1983, pp. 61-70.

7. Cheeseman, I.C., Haddow, C., "An Experimental Investigation of the Downwash Beneath a Lifting Rotor and Low Advance Ratios," *Vertica*, Vol. 13, No. 4, 1989, pp. 421-445.

8. Biggers, J.C., Orloff, K.L., "Laser Velocimeter measurements of the Helicopter Rotor Induced Flowfield," Proceedings of the *30th Annual Forum of the American Helicopter Society*, Washington D.C., May 7-9, 1974.

9. Althoff, S.L., Elliott, J.W., Sailey, R.H., "Inflow Measurements made with a Laser Velocimeter on a Helicopter Model in Forward Flight," NASA Technical Memorandum 100544, April 1988.

10. Brand, A.G., McMahon, H.M., Komerath, N.M., "Wind-Tunnel Data from a Rotor Wake/Airframe Interaction Study," Data Report No. GITAER 87-1, School of Aerospace Engineering, Georgia Institute of Technology, July 1986.

11. Earnshaw, P.B., "An Experimental Investigation of the Structure of Leading Edge Vortex," R.A.E. Technical Note No. Aero. 2740, 1961.

12. Leishman, J.G., Bi, Nai-pei, Samak, D.K., Green, M., "Investigation of Aerodynamic Interactions between a Rotor and a Fuselage in Forward Flight," Proceedings of the *45th Annual Forum of the American Helicopter Society*, Boston, Mass., May 21-24, 1989. To appear in AHS Journal, July 1990.

13. Bi, Nai-pei, Leishman, J.G., "Experimental Study of Aerodynamic Interactions between a Rotor and a Fuselage," Paper 89-2211, *AIAA 7th Applied Aerodynamics Conference*, Seattle, WA, July 31-Aug. 2, 1989. To appear in AIAA Journal of Aircraft, 1990.

14. Crouse, G.L., Leishman, J.G., Bi, Nai-pei, "Theoretical and Experimental Study of Unsteady Rotor/Body Aerodynamic Interactions," Proceedings of the *46th. Annual Forum of the American Helicopter Society*, Washington D.C., May 21-23, 1990.

15. Gerner, A.A., Maurer, C.L., "Calibration of Seven-Hole Probes Suitable for High Angles in Subsonic Compressible Flows," U.S. Air Force Academy, Colorado Springs, Report USAFA-TR-81-4, 1981.

16. Gerner, A.A., Maurer, C.L., Gallington, R.W., "Non-nulling Seven Hole Probes for High Angle Flow Measurement," *Experiments in Fluids*, Vol. 2, 1984, pp. 95-103.

17. Wilson, J.C., Mineck, R.E., "Wind-Tunnel Investigation of Helicopter Rotor Wake Effects on Three Helicopter Fuselage Models," NASA TM X-3185, 1975.

18. Smith, C.A., Betzina, M.D., "Aerodynamic Loads Induced by a Rotor on a Body of Revolution," *Journal of the American Helicopter*, Vol. 31, No. 1, Jan. 1986, pp. 29-36.

19. Heyson, H.H., "Preliminary Results from Flow-Field Measurements around Single and Tandem Rotors in the Langley Full-Scale Tunnel," NACA TN 3242, 1954.

20. Cooper, D.E. "YUH-60A Stability and Control," *Journal of the American Helicopter Society*, Vol. 23, No. 3, July 1978, pp. 2-9.